Design and Optimization of Dielectric DBR for VCSEL, Targeting Emission Range of 520-550 nm

Romal Kumar, Karansingh Thakor, Shaurya Gupta, Raghupathi Maripeddi, Dhiman Nag, Apurba Laha

Abstract—The report stresses on the optimization of dielectric Distributed Bragg Reflector (DBR) for Vertical Cavity Surface Emitting Laser (VCSEL) for emission range of 520-550 nm. DBR plays an important role in the efficiency of VCSELs. Transfer Matrix Method (TMM) was used to design the model for propagation and interface matrix. Power reflectance was calculated for various Ta_2O_5 and SiO_2 DBR stack pairs with varying wavelength that will travel through the stack and is studied thoroughly. The simulation was done using MATLAB® to see the stop-band variation with stack pairs. The thickness of a DBR pair was kept constant during the simulation. The result yields power reflectance above 90% for DBR stack pair greater than 6 and saturates for stack pair more than 16. The simulation was done for normal incidence which produces promising results.

Index Terms—Dielectric Distributed Bragg Reflector, Vertical Cavity Surface Emitting Laser, Reflectance, Transfer Matrix Method, MATLAB® Simulation

1 Introduction

THE idea of a laser was first predicted by Albert Einstein in his paper *Zur Quantentheorie der Strahlung* (On the Quantum Theory of Radiation) in 1917. It took some time till lasers were explored in more detail and pioneering works were done on making masers (Microwave Amplification by Stimulated Emission Radiation). Soon in the late 1950s the field of lasers took up and has been an emerging field even today [1]. Lasers have found tremendous applications in various fields of technology, devices and in the field of medicine. They have also found profound uses as an hobby for many people across the world.

The concept of VCSELs (Vertical Cavity Surface Emitting Lasers) were first conceptualized by Prof. Kenichi Iga in 1977. The VCSEL device has seen various publications over the years and people are still looking for potential applications of it. They have found uses in high speed optical data transmission and uses in an optical mouse. The number of VCSELs produced annually is about 100 million and are next to Fabry-Pérot type *edge-emitting lasers* (EELs) [2]. A schematic of a VCSEL is shown in Fig:1.

The growth of a VCSEL requires very high quality and precision growth, so growth techniques like MBE (Molecular Beam Epitaxy) or MOCVD (Metal-Organic Chemical Vapour Deposition) are often employed when fabricating a VCSEL. VCSELs emitting light in the wavelength region of 850-980 nm require about 8 μm of *epitaxial* growth (as indicated in Fig:1). The inner cavity and the active layer comprises of a Multi-Quantum Well (MQW) structure and just spans about 10 nm in thickness.

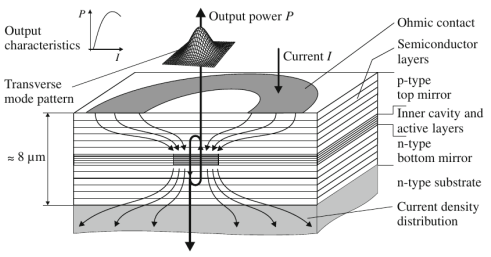

Fig. 1: Schematic layer structure of a VCSEL

1.1 Basics of Laser

Laser (more accurately *LASER*) is an acronym for Light Amplification by Stimulated Emission Radiation.

A set of simplified governing equations that explain the working principle of a laser are written below:

Let R_{sp}, R_{abs} and R_{st} denote the rates for spontaneous emission, absorption and stimulated emission respectively. As a first order approximation

- *Prof. Apurba Laha is at the Department of Electrical Engineering at the Indian Institute of Technology, Bombay.*
  E-mail: laha@ee.iitb.ac.in
- *Mr. Dhiman Nag is currently a PhD student in the Department of Electrical Engineering at the Indian Institute of Technology, Bombay.*
- *The rest of them are students at the Indian Institute of Technology, Bombay.*

Report submitted April 27, 2019; revised N.A. as of now

and related by proportionality constants, the respective rates should depend on the electron concentration of those levels which are involved for the observed phenomena [3].

$$\begin{aligned} R_{sp} &= A_{sp} N_1 \\ R_{abs} &= B_{abs} N_2 \phi \\ R_{st} &= B_{st} N_1 \phi \end{aligned} \tag{1}$$

where: A_{sp}, B_{abs}, B_{st} are called the Einstein coefficients. N_1 and N_2 are the electron concentrations at the energy levels, E_1 and E_2 respectively as shown in Fig: 2. ϕ is the intensity of laser light generated.

In a radiative equilibrium: number of photons must be conserved.

$$\text{Hence, } R_{abs} = R_{sp} + R_{st}$$

The Einstein coefficients for the absorption and stimulated radiation for equal.

$$\text{Hence, } B_{abs} = B_{st} = B \text{ (say)}$$

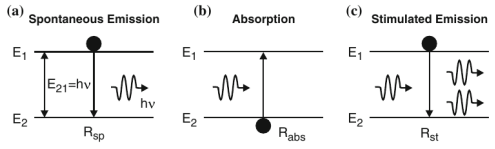

Fig. 2: Principle of Laser ≡ Light Amplification by Stimulated Emission Radiation

In a laser mode, spontaneous emission can be neglected.

$$\therefore\ R_{st} - R_{abs} = (N_1 - N_2) B \phi \tag{2}$$

It can be seen that there is net light amplification whenever $R_{st} > R_{abs}$, i.e., when $N_1 > N_2$ or in other words when one achieves a *population inversion*. The above formulation also shows the importance of light amplification intensity, ϕ, higher the amplification we achieve, higher is the output from the laser; given that *population inversion* has been achieved. This fact will be central when designing and optimizing a Distributed Bragg Reflector (DBR) stack.

1.2 Distributed Bragg Reflector (DBR)

VCSEL, as the name reads out corresponds to the light emission along the vertical cavity surface of the device and these devices are of nanometer scales. Hhence, it's crucial that we get high optical gain length to achieve significant light amplification. The gain length for optical amplification in a Fabry-Pérot type laser is of the order of few micrometers. This makes it necessary to have reflecting surfaces stacked around the active region (MQW) of a VCSEL.

Optical gain length in a VCSEL is simply the accumulated thickness of the MQW structure. About 5 MQWs are used and this leads to a optical gain length of about 20 nm. If only MQWs are emplyed for light amplification, this length is too small to get any appreciable laser light intensity. Hence it puts the constraint of having near perfect total reflectance ($\approxeq 100\%$) of the entire reflecting mirror assembly. All practical implementations of the mirror assembly have more than 97% reflectance.

The optical confinement of light in a VCSEL is achieved by using a *Distributed Bragg Reflector* (DBR). A DBR stack is a multi layered structure of alternating high and low refractive index layers. The thickness of each individual layer is $\lambda/4$, where λ is the wavelength of light that will be generated in the Multi-Quantum Well (MQW). The light intensity is amplified as it is reflected back and forth in the stack of reflecting mirrors around the active region. Semiconductor and dielectric DBRs are typically used to confine light in longitudinal direction. One could in principle also use High-Contrast Gratings (HCG) but it is not a practically feasible approach and instead one uses a DBR.

The explanation for $\lambda/4$ thickness of each layer is presented below (or could have as well written as an appendix text).

A DBR stack employed on either side of the active region has many layers of the material and this then leads to consider how thick each layer should be so that we get constructive interference. The DBR arrangement involves alternating layers of high and low refractive index materials. There is a phase change of π when light is reflected from material of higher refractive index incident from a lower refractive index material. There is a phase change of 2π ($\equiv 0$) when light is reflected from material of lower refractive index incident from a higher refractive index material. Also, we consider near-normal incidence light reflections and transmissions.

We have,

$$\Delta\phi = \frac{2\pi}{\lambda} d \cdot n$$

where, $\Delta\phi$ is the phase change due to propagation of light with wavelength λ along a geometric distance d in a medium of refractive index with real component n.

Now the following effects are taken into account, the phase change due to reflection from higher or lower refractive index materials and the phase change due to propagation. Using this one derives the conditions for constructive and destructive interference when each layer has a thickness of $\lambda/4$ (as shown in Fig: 3), where λ is the wavelength of the light which the device would be generating.

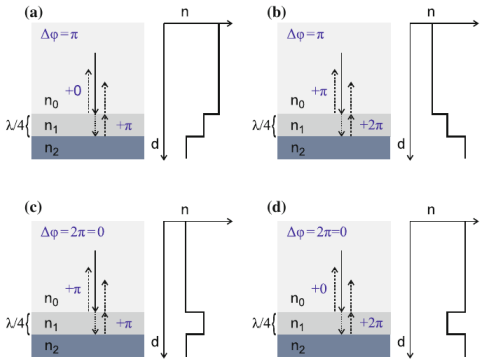

Fig. 3: Various interference situations

In Fig: 3, for the (b) part [note that (a) and (b) can be explained by *similar* reasoning, here we explain part (b)]: the thickness of each layer is $\lambda/4$ and there is phase shift of π because $n_1 > n_0$ and there is a phase of shift of π again due to reflection at n_2 since $n_2 > n_1$ and a further phase difference of π due to optical length. So, there is a net phase difference of $2\pi - \pi = \pi$ when the rays after reflection at n_1 and n_2 occur. This results in a destructive interference. But, this was the case when there wasn't any alternations in the refractive index sequences.

In Fig: 3, for the (d) part [note that (c) and (d) can be explained by *similar* reasoning, here we explain part (d)]: observe that the refractive index of a pair of layers alternate – by which we mean that the refractive indices of the materials alternate between high and low value by using suitable materials. Here, there is no phase change when there is reflection at n_1 because $n_0 > n_1$ and there is a phase change of π due to reflection at n_2 because $n_2 > n_1$, and on top of that there is an optical phase shift of $\pi \left(= \frac{\pi}{2} + \frac{\pi}{2}\right)$. This leads to a total phase shift of $2\pi(\equiv 0)$ when the reflected rays from n_0 and n_2 interfere. This results in a constructive interference.

Hence, it is proved that thickness of each layer should be $\lambda/4$ in order to have constructive interference and make sure that the light intensity doesn't diminish due to destructive interference. Also, it can be concluded that the refractive indices of the constituting materials should be arranged in an alternating sequence.

At the same time, there are $\lambda/2$ layers inserted between DBR stacks of no optical activity known as absentee layers which serve as contact layers. $\lambda/2$ is chosen because this doesn't contribute to phase difference due to optical path length, and on top of that there is no phase change due to reflection because the layer doesn't have any optical activity.

As there is a possibility of multiple reflections to occur and there is a series of DBR pairs, the criteria for constructive interference for a range of wavelengths centered around λ get satisfied, so there is a notion of stop band.

Stop band is defined as width between two wavelengths where DBR power reflectance has dropped to 90%. The width of the stop band reduces with more and more number of absentee layers. Width of the stop band (which in absence of absentee layer is about 50-100 nm) is important because that gives the error margin one can have in fabricating the thickness of the QW (which would decide λ); the lesser the stop band width is, more fine tuning of the QW thickness is required so that the wavelength of the laser light produced in the active region lies between high-reflectance wavelengths of the DBR stack implemented. The stop band for our purpose has to be between 520-550 nm.

1.3 Types of DBR

DBRs can be of three types: epitaxial, dielectric and air-gap based.

III-nitrides materials are preferred for DBRs because of:

- ease of fabrication and growth
- can fabricate materials to obtain sufficient index contrast between $\lambda/4$ layers
- better thermal conductivity

Poor electrical conductivity and high absorption losses in p-type III-Nitrides has led to use of dielectric DBRs for p-side of the device. [4]

Use of epitaxial n-side and dielectric p-side forms a hybrid DBR VCSEL. On the other hand, dielectric p and n DBR are dual-dielectric DBR VCSEL. Epitaxial DBR have smaller index contrast. Since the index contrast is smaller, one requires more periods of epitaxial n-DBR and more periods leads to smaller stop band widths.

Approximately, an epitaxial DBR has a stop band width of about 35 nm and a dielectric DBR has a stop band width of about 70 nm.

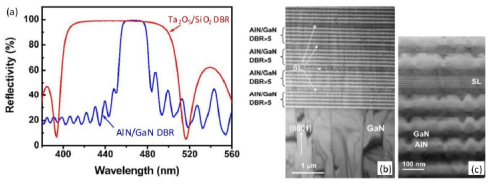

Fig. 4: Reflectivity Spectrum for Ta_2O_5/SiO_2 dielectric p-DBR and AlN/GaN epitaxial n-DBR and the other two are TEM images of the AlN/-GaN stack

The figure Fig: 4 shows reflectivity spectrum for Ta_2O_5/SiO_2 dielectric p-DBR and AlN/GaN epitaxial n-DBR on a 450 nm c-plane VCSEL.

The TEM images indicate formation of superlattice structure. This prevents cracking caused by large lattice mismatch between AlN and GaN layers. There is significant interface roughness which will contribute to scattering loss in VCSEL. Also, it can be seen from the reflectance spectra (stop band) centered around 450 nm is wider for Ta_2O_5/SiO_2 which is a dielectric DBR as opposed to a narrower stop band seen for an epitaxial n-DBR (AlN/GaN stack).

For the choice of materials for an epitaxial DBR, AlN/GaN stack is difficult to grow because of high lattice mismatch between AlN/GaN and leads to catastrophic cracking. AlInN/GaN stack is difficult to grow but by using concept of buffer layer, once the stack is fabricated, it is free from internal stresses. Superlattice structures were found in the grown DBR stack (GaAs/AlAs). [5]

Again, it can be seen from Table: 1 that thermal conductivity of dielectric materials like Ta_2O_5 and SiO_2 is very less as compared to epitaxial III-nitrides like GaN or AlN. Dealing with thermal aspects are important as the lifetime of the device is governed by how well the thermal stresses are handled and how well the thermal energy is dissipated (note that it is has to along the vertical cavity as there is no appreciable lateral dissipation). An air-gap has even much lesser thermal conductivity than a dielectric material.

Material	Thermal Conductivity (W/cm-K)
GaN	1.3
AlN	2.85
ITO	0.05
Ta_2O_5	0.0045
SiO_2	0.007
Au	3.17

TABLE 1: Thermal conductivities for some materials that are used in DBR

Interface roughness caused by V-defects in c-plane growth leads to scattering of light and causes local variations. In total, it reduces the reflectance of the mirror.

Dielectric DBR can be fabricated using sputtering techniques. MOCVD and MBE techniques are not necessary. But, very high degree of control and precision is required because we want to avoid interface roughness and moreover sputtering techniques require longer time duration (about 6-12 hours). During the fabrication process, there are complicated membrane liftoff and bonding processes involved. So, dielectric DBRs are difficult to fabricate and grow than an epitaxial DBR. Ion beam deposition can be used but, it's an expensive setup.

At the same time, dielectric DBRs have lower thermal conductivity than an epitaxial III-nitride DBR. For a dielectric DBR, one needs to rely on lateral dissipation of heat generated.

A properly optimized dual dielectric DBR will have better thermal and an overall performance than a hybrid DBR (int terms of reflectivity and stop band width).

There isn't enough of contrast between epitaxial DBR - for example, $n_{GaN}/n_{AlN} = 2.7/2.15$ for photons with energy, $E = 3.4ev$. It can be seen that the Δn ($= 0.55$) is not *very high*. [6]

For a DBR that uses air-gap microcavity (formed by say decomposition of GaN) - it has been found that 3 top DBRs and 4 bottom DBRs are sufficient and since less number of DBRs are used, there is less growth error overall. But, the problem is on the thermal side, air-gap doesn't have high thermal conductivities and the application would be limited to low power VCSELs unless proper optimization is done [7].

For the ITO (Indium Tin Oxide) and TJ (Tunneling Junction) VCSEL, after certain number of p-DBR pairs, there wasn't any appreciable change in the reflectance spectra around the centered wavelength. After 10 to 12 p-DBR mirror periods, there wasn't any appreciable change in the reflectance spectra though the reflectance spectra was already appreciable even with 2 p-DBR mirror periods. Whereas for an epitaxial n-DBR, the stop band width gets progressively lesser with number of mirror periods and to get appreciable power reflectance, there is need for around 20-22 epitaxial n-DBR mirror periods.

Apart from this, in the literature survey done pertaining to other *references* given in [8] (not directly to do with dielectric DBR) has been stated from here on.

GaN-based air-gap DBR were fabricated using band-gap selective photoelectrochemical etching as described in [9].

Optimizations were done based on chemical composition as well. In particular, thermal resistivity of $In_{1-x}Ga_xAs_yP_{1-}y$ was found to be maximum when $y = 0.75$ and the value of thermal conductivity at that y was 24 $W^{-1}cmK$ [10].

Improvements were observed in the laser performance by reduction of acceptor concentration in the p-type mirror of the VCSEL. For Nitride based light emitting devices, low activation ratio of p-type (Al)GaN were observed by doping with Magnesium (Mg) to activate the acceptors [11].

2 Transfer Matrix Method

Transfer Matrix Method (TMM) is a generalized approach in treatment of multilayered optical materials [12].

Consider a 3-layered material as shown in Fig:5 with a refractive index profile (wrt to the coordinate system shown) [13].

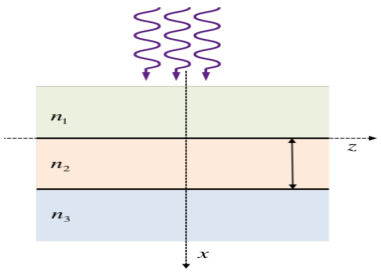

Fig. 5: Light incident on a multi-layered structure

$$n(x) = \begin{cases} n_1, & x < 0 \\ n_2, & 0 < x < d \\ n_3, & x > d \end{cases} \tag{3}$$

We create a matrix D_{12} which is the interface matrix for travelling from material-1 of refractive index n_1 to a material-2 of refractive index n_2. We assume the normal incidence.

$$D_{12} = \begin{pmatrix} \frac{n_2+n_1}{2n_2} & \frac{n_2-n_1}{2n_2} \\ \frac{n_2-n_1}{2n_2} & \frac{n_2+n_1}{2n_2} \end{pmatrix}$$

Then we multiply with the phase propagation matrix while the wave travels in material-2 of refractive index n_2.

$$P_2 = \begin{pmatrix} e^{ik_{2x}d} & 0 \\ 0 & e^{-ik_{2x}d} \end{pmatrix}$$

Similarly, we can find the matrix for the light going from material-2 of refractive index n_2 to material-3 of refractive index n_3 which will be D_{23} as follows. The column vector on the left side of the equation below is the input and the column vector on the right side is the output [13].

$$D_{23}P_2D_{12}\begin{pmatrix} E_1 \\ E_1' \end{pmatrix} = \begin{pmatrix} E_3 \\ E_3' \end{pmatrix}$$

2.1 Periodic Medium

We apply similar logic to the periodic system with pairs of dielectrics with refractive indices n_1 and n_2. Consider the light flowing from material-2 to material-1. Using the similar strategy from the previous section the transfer matrix for light travelling from material-2 to material-1 can be written as:

$$E_{in} = D_{21}P_2E'_{out}$$

Similarly looking at the interface for material-1 to material-2:

$$E'_{out} = D_{12}P_1E_{out}$$

Hence,

$$E_{in} = D_{21}P_2D_{12}P_1E_{out}$$

Therefore, the transfer matrix can be written as:

$$M = D_{12}P_2D_{12}P_1$$

Note that, E_{in}, E_{out} and E'_{out} are all 2×1 matrices with both the incident and reflected components in them.

In a DBR stack, there will be 'N' number of pairs of dielectrics DBR layers with different dielectrics constants. They will be put on a substrate as shown in the Fig:6.

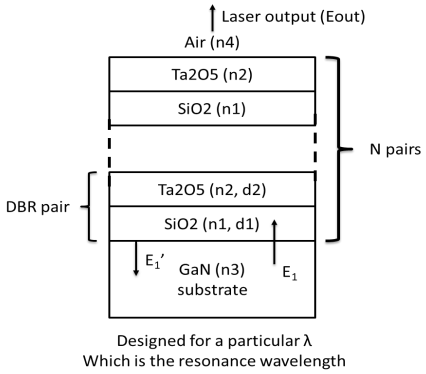

Fig. 6: Schematic of a DBR stack with substrate

The final transfer equation will be written as:

$$M_{final} = D_{24}\cdot(M^N)\cdot D_{31}\cdot P_1$$

$$M_{final} = \begin{pmatrix} M_{11} & M_{12} \\ M_{21} & M_{22} \end{pmatrix}$$

As E_{out} has only forward propagating component but E_{in} has both forward and backward components, which is found using the equation:

$$\begin{pmatrix} E_{in} \\ E'_r \end{pmatrix} = \begin{pmatrix} M_{11} & M_{12} \\ M_{21} & M_{22} \end{pmatrix}\cdot\begin{pmatrix} E_{out} \\ 0 \end{pmatrix}$$

Now the reflectance, r, is given by the ratio of the M_{11} and M_{21} coefficients of M_{final},

$$r = \frac{E_r}{E_{in}} = \left|\frac{M_{21}}{M_{11}}\right|$$

3 TMM code in MATLAB

```
%TMM.m
clear all;
%R.I.
n1 = 1.5; % SiO2
n2 = 2.16; % T2O5
n3 = 2.37; % GaN
n4 = 1;   % Air

N = 32;     % DBR pairs
lo = 500e-9; % resonance wavelength, nm
i = 1;

for l = 300e-9 : 0.1e-9 :800e-9
```

```
    k1 = (2*pi*n1)/l;
    d1 = lo/(4*n1);
    p1 = k1*d1;

    k2 = (2*pi*n2)/l;
    d2 = lo/(4*n2);
    p2 = k2*d2;

    A1 = (n2+n1)/(2*n2);
    A2 = (n2-n1)/(2*n2);
    A3 = (n1+n2)/(2*n1);
    A4 = (n1-n2)/(2*n1);

    D12 = [A1 A2 ; A2 A1];
    D21 = [A3 A4 ; A4 A3];

    P1 = [exp(1j*p1) 0 ; 0 exp(-1j*p1)];
    P2 = [exp(1j*p2) 0 ; 0 exp(-1j*p2)];

    M = D21*P1*D12*P2;
    Mn = M^N;

    %GaN and SiO2

    k1 = (2*pi*n1)/l;
    d1 = lo/(4*n1);
    p1 = k1*d1;

    A3 = (n1+n3)/(2*n3);
    A4 = (n1-n3)/(2*n3);

    D31 = [A3 A4 ; A4 A3];

    P1 = [exp(1j*p1) 0 ; 0 exp(-1j*p1)];

    %Ta2O5 and air

    A3 = (n2+n4)/(2*n4);
    A4 = (n2-n4)/(2*n4);

    D24 = [A3 A4 ; A4 A3];

    Mf = D24*Mn*D31*P1;

    r(i) = abs(Mf(2,1)/Mf(1,1));
    l1(i) = l;

    i = i+1;
    plot(l1,r);
    hold on;
end
```

4 Results

The simulation of the DBR stack was implemented using the Transfer Matrix Method and the code was executed in MATLAB®. The aim was to obtain reflectance spectra targeting emission range of 520-550 nm. The aim is clear here, as stated in the extensive introduction section of this report/paper, dielectric DBR stack gives the widest stop-band and moreover the reflectivity is very constant in the stop-band region. The performance of a dielectric DBR when compared to that of an epitaxial DBR as shown in Fig:4 clearly indicates that a dielectric DBR is preferred over an epitaxial DBR.

In our simulation, we have a GaN substrate having a refractive index (for now, we don't consider the complex part of the refractive index) of 2.37 for the wavelengths in between 500-550 nm. The DBR pair consists of Ta_2O_5 and SiO_2 of refractive indices 2.16 and 1.5 respectively. The two types of layers are arranged in alternating pattern and stacked on top of each other. The graphs, Reflectance spectra (and also the stop-band) vs wavelength are shown in Fig:7 and Fig:8 considering different number of DBR pairs 'N', as indicated in the legend of the graphs.

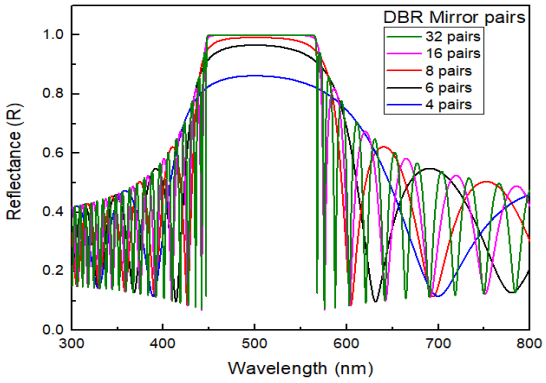

Fig. 7: Reflectance spectra vs wavelength

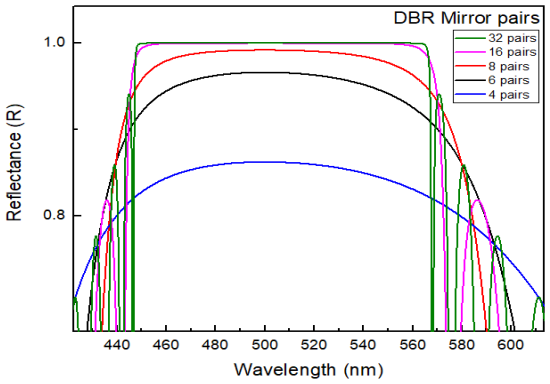

Fig. 8: Reflectance spectra vs wavelength centered around 520-550 nm

5 Conclusions

Transfer Matrix Method has been successfully implemented to calculate the reflectance spectra of a multi-layered arrangement of consisting of two materials. The simulation results justify that making a dielectric DBR stack for VCSEL targeting emission in the range of 520-550 nm is very much possible with the use of materials like SiO_2 and Ta_2O_5, which are dielectrics.

The material pair for the DBR stack can be used for actually making the VCSEL. Also, the optimum number of DBR can be taken to between 8 to 16 pairs. As of now, the distribution of the DBR stack is symmetric about the active layer of the VCSEL. It is observed from the graphs,

Fig:7 and Fig:8 that the reflectance value and the stop-band vs wavelength have saturated after 8 to 16 DBR pairs. It is remarkable that the stop-band didn't become more narrow as the DBR pairs were increased to 32 but, the stop-band would have reduced in width if it were an epitaxial DBR. We have also achieved the reflectivity (or power reflectance) of around 100%, which is the requirement in case of a VCSEL for DBR pairs between 8 to 16.

6 Future Work

We haven't considered any absentee layer in the DBR stack. Though, the absentee layer doesn't affect the reflectance spectra ideally but considering those layers which are very much present in an actual fabrication, we can make fine tuning to the reflectance and stop-band spectra which we obtained.

Analyze the heat transfer across the DBR stack because one of the disadvantage of a dielectric DBR is its poor thermal conductivity. In order to keep the device healthy, thermal management analysis should be critically evaluated. Getting to know the environment in which our device will be used, we can find thermal profile around the device and then look into what actions might need to be done.

References

[1] M. Bertolotti, *Masers and Lasers: An Historical Approach*. CRC Press, 2015.

[2] R. Michalzik, *VCSELs: Fundamental, Technology and Applications of Vertical-Cavity Surface-Emitting Lasers*, 1st ed. Springer Berlin Heidelberg, 2013.

[3] P. Moser, *Energy-Efficient VCSELs for Optical Interconnects*. Springer Theses, 2016.

[4] E. Kioupakis, P. Rinke, and C. G. Van de Walle, "Determination of internal loss in nitride lasers from first principles," *Appl. Phys. Express*, vol. 3, 2010.

[5] G. Huang, T. Lu, H. Yao, H. Kuo, S. Wang, C. Lin, and L. Chang, "Crack-free gan/aln distributed bragg reflectors incorporated with gan/aln superlattices grown by metalorganic chemical vapor deposition," *Appl. Phys. Lett.*, vol. 88, pp. 5–7, 2006.

[6] T. Lu, J. Chen, T. Wu, P. Tu, C. Chen, C. Chen, Z. Li, H. Kuo, and S. Wang, "Continuous wave operation of current injected gan vertical cavity surface emitting lasers at room temperature," *Appl. Phys. Lett.*, vol. 97, 2010.

[7] T. R., A. M., K. S., and A. Y., "Fabrication and optical properties of non-polar iii-nitride air-gap distributed bragg reflector microcavities," *Appl. Phys. Lett.*, vol. 103, 2013.

[8] J. T. Leonard, "Iii-nitride vertical-cavity surface-emitting lasers," Ph.D. dissertation, University of California - Santa Barbara, 2016.

[9] R. Sharma, E. Haberer, C. Meier, E. Hu, and S. Nakamura, "Vertically oriented gan-based air-gap distributed bragg reflector structure fabricated using band-gap-selective photoelectrochemical etching," *Appl. Phys. Lett.*, vol. 87, 2005.

[10] T. Ashida, A. Miyamura, N. Oka, Y. Sato, T. Yagi, N. Taketoshi, T. Baba, and Y. Shigesato, "Thermal transport properties of polycrystalline tin-doped indium oxide films," *J. Appl. Phys.*, vol. 105, 2009.

[11] W. Götz, N. Johnson, J. Walker, D. Bour, and S. R.A., "Activation of acceptors in mg-doped gan grown by metalorganic chemical vapor deposition," *Appl. Phys. Lett.*, vol. 68, 1996.

[12] C. C. Katsidis and D. I. Siapkas, "General transfer-matrix method for optical multilayer systems with coherent, partially coherent, and incoherent interference," *Appl. Opt.*, vol. 41, no. 19, pp. 3978–3987, Jul 2002. [Online]. Available: http://ao.osa.org/abstract.cfm?URI=ao-41-19-3978

[13] M. OpenCourseWare, "Lecture 23 - layered materials and photonic band diagrams," https://ocw.mit.edu/courses/materials-science-and-engineering/3-024-electronic-optical-and-magnetic-properties-of-materials-spring-2013/lecture-notes/MIT3_024S13_2012lec23.pdf, accessed: 26 April 2019.